Aalborg Universitet

AALBORG UNIVERSITY

Sensorless Suitability Analysis of Hybrid PM Machines for Electric Vehicles

Matzen, Torben Nørregaard; Rasmussen, Peter Omand

Published in:
Proceedings of the International Conference & Exhibition on Ecologic Vehicles & Renewable Energies (EVER 09)

Publication date:
2009

Document Version
Publisher's PDF, also known as Version of record

Link to publication from Aalborg University

Citation for published version (APA):
Matzen, T. N., & Rasmussen, P. O. (2009). Sensorless Suitability Analysis of Hybrid PM Machines for Electric Vehicles. In *Proceedings of the International Conference & Exhibition on Ecologic Vehicles & Renewable Energies (EVER 09)* University of Sfax, Tunisia.

General rights
Copyright and moral rights for the publications made accessible in the public portal are retained by the authors and/or other copyright owners and it is a condition of accessing publications that users recognise and abide by the legal requirements associated with these rights.

- Users may download and print one copy of any publication from the public portal for the purpose of private study or research.
- You may not further distribute the material or use it for any profit-making activity or commercial gain
- You may freely distribute the URL identifying the publication in the public portal -

Take down policy
If you believe that this document breaches copyright please contact us at vbn@aub.aau.dk providing details, and we will remove access to the work immediately and investigate your claim.

Downloaded from vbn.aau.dk on: June 04, 2025

Sensorless Characteristics of Hybrid PM Machines at Zero and Low Speed

Torben N. Matzen and Peter O. Rasmussen
Aalborg University - Institute of Energy Technology
Pontoppidanstraede 101
DK-9220 Aalborg East, Denmark
Email: {tnm,por}@iet.aau.dk

***Abstract*—Sensorless methods for zero and low speed operation in drives with hybrid PM machines make use of the machine saliency to determine the rotor position in an indirect fashion.**

When integrating the position measurement in the electrical power supply to the machine, i.e. make the machine self-sensing, the sensorless obtained position can be affected by the actual operation conditions of the machine e.g. the stator currents. This may deteriorate the machine self-sensing suitability using injection methods.

In this paper an analysis method based on accurate knowledge of the machine flux linkages is proposed for analysing the suitability for sensorless control at zero and low speed.

The method can be used to evaluate a particular machine design so the self-sensing characteristics for sensorless control of machine can be found. The characteristics can be obtained from finite element simulation data or experimental data.

I. Introduction

Hybrid PM machines are interesting due to the possibility of achieving a high efficiency and the design freedom in combining permanent magnet (PM) and reluctance torque components to achieve torque-speed characteristics well suited for a specific application e.g. automotive traction applications. [1]

Sensorless control for traction machines is interesting from a fail safe point of view which could replace an exposed mechanical sensor, act as supervision or as backup for limp home operation. In addition incremental mechanical sensors has an inherent undefined initial position, where sensorless injection methods may be used for initial position detection.

The rotor position is determined by means of injection signals separated in frequency from the fundamental driving voltage and current. In literature different zero/low speed sensorless methods has been proposed which all rely on tracking the rotor position dependent inductance. [2]–[7]

The apparent inductance may vary due to magnetic saturation caused by the applied stator currents and the geometrical layout of the rotor and stator. These phenomena may deteriorate the suitability for low and zero speed sensorless control. Hence, an accurate knowledge of the machine in particular the inductance is very relevant to obtain, to analyse in advance the suitability of a machine for sensorless control. The paper considers only the sensorless characteristics of the machine without the need to know what type of sensorless injection based method is used, as long as the method rely on the inductance properties of the machine.

II. Electrical Machine Model

The linear electrical dq-model of salient PM machine can be described by the following governing differential voltage equation and flux linkage equation

$$\begin{bmatrix} v_d \\ v_q \end{bmatrix} = \begin{bmatrix} R & 0 \\ 0 & R \end{bmatrix} \begin{bmatrix} i_d \\ i_q \end{bmatrix} + \frac{\mathrm{d}}{\mathrm{d}t} \begin{bmatrix} \lambda_d \\ \lambda_q \end{bmatrix} + \omega_r \begin{bmatrix} -\lambda_q \\ \lambda_d \end{bmatrix} \quad (1)$$

$$\begin{bmatrix} \lambda_d \\ \lambda_q \end{bmatrix} = \underbrace{\begin{bmatrix} L_{dd} & L_{dq} \\ L_{qd} & L_{qq} \end{bmatrix}}_{\boldsymbol{L}} \begin{bmatrix} i_d \\ i_q \end{bmatrix} + \begin{bmatrix} \lambda_{PM} \\ 0 \end{bmatrix}, \quad (2)$$

where R is the stator resistance, ω_r the shaft speed, L_{dd} and L_{qq} the d-, q-axis inductance, L_{dq} and L_{qd} cross inductance and λ_{PM} the PM flux linkage.

The linear salient dq-model has zero cross inductance ($L_{dq} = L_{qd} = 0\,\mathrm{H}$) and constant d- and q-axis inductances which are different so the machine has an inductance saliency ratio $\frac{L_{qq}}{L_{dd}} > 1$ and then the rotor position θ_r can be tracked using injection methods. However due to the magnetic saturation phenomenon in electrical steels used for manufacturing electric machines, the cross inductance may become different from zero and the inductance parameter matrix $\boldsymbol{L}$ can not be assumed to be constant [8].

The varying inductance matrix gives a more complex behaviour of the machine which may affect the suitability of the machine for sensorless control.

The following two functions is a more detailed representation of the flux linkage instead of (2).

$$\begin{bmatrix} \lambda_d \\ \lambda_q \end{bmatrix} = \begin{bmatrix} \lambda_d(i_d, i_q, \theta_r) \\ \lambda_q(i_d, i_q, \theta_r). \end{bmatrix} \quad (3)$$

The functions describe the dq-flux linkage which in this case is restricted to be dependent on the dq-currents to include saturation effects and rotor position θ_r to include possible spatial flux linkage harmonics. The flux linkage dependence on the rotor position θ_r is considered to include possible harmonic components which could originate form e.g. stator slots, rotor geometry and winding layout.

It is assumed that the flux linkage including inductance is independent of frequency up to some limit where the applied

injection signals contains frequencies below this limit. The PM strength is sensitive to temperature and may also decay over time, which will affect the dq-flux linkage. Here the PM strength is considered constant.

The flux linkage functions are the basis for the suitability analysis proposed in this paper. In practise the functions in (3) could be data sets from either finite element method simulations of a machine design or from experimental characterisation of an existing machine.

From the flux linkage functions the apparent inductance may be found and is defined as

$$\boldsymbol{L}(i_d, i_q, \theta_r) \quad = \quad \begin{bmatrix} \frac{\partial \lambda_d}{\partial i_d} & \frac{\partial \lambda_d}{\partial i_q} \\ \frac{\partial \lambda_q}{\partial i_d} & \frac{\partial \lambda_q}{\partial i_q} \end{bmatrix}, \tag{4}$$

which is a function of the dq-current and rotor position.

From this inductance matrix important characteristics for sensorless control which are the saliency ratio and saliency direction is introduced in the following subsection.

A. Saliency Ratio and Direction

To clarify the meaning of saliency ratio and direction the impact of the inductance matrix $\boldsymbol{L}$ which relates the small-signal dq-current to the flux linkage is shown in Fig. 1 neglecting the PM-flux linkage contribution. From the figure

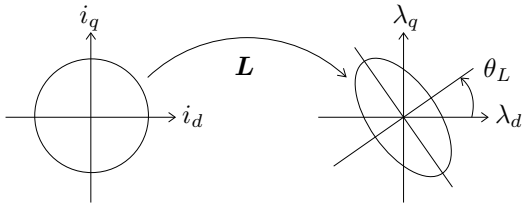

Fig. 1. Inductance matrix $\boldsymbol{L}$ transformation.

the saliency ratio is the ratio between the major and minor ellipse axis. The angle of the ellipse is indicated by θ_L, which is denoted the saliency angle. To obtain the ratio and angle of the inductances in the machine singular value decomposition (SVD) is applied on the inductance matrix $\boldsymbol{L}(i_d, i_q, \theta_r)$. Using SVD the inductance is decomposed into two orthogonal and one singular matrix as

$$\boldsymbol{L} \quad = \quad \boldsymbol{U}\boldsymbol{\Sigma}\boldsymbol{V}^T, \tag{5}$$

where $\boldsymbol{U}$ and $\boldsymbol{V}$ are orthogonal containing the axis direction and $\boldsymbol{\Sigma}$ is singular containing the ratio. [9]

From the decomposition the major, minor inductance and saliency angle are introduced as

$$\boldsymbol{\Sigma} \quad = \quad \begin{bmatrix} L_{\text{major}} & 0 \\ 0 & L_{\text{minor}} \end{bmatrix} \tag{6}$$

$$\boldsymbol{U} \quad = \quad \begin{bmatrix} -\sin(\theta_L) & \cos(\theta_L) \\ \cos(\theta_L) & \sin(\theta_L) \end{bmatrix} \tag{7}$$

where θ_L is the saliency angle in the dq-frame so the saliency direction $\theta_{\hat{r}}$ in the stator frame is the rotor position including the saliency angle (error) relative to the dq-frame

$$\theta_{\hat{r}} = \theta_r + \theta_L. \tag{8}$$

When cross coupling occurs the saliency direction is no longer coincident with the d-axis, the direction of the saliency axis is where the minimum inductance is observed. Also the true saliency ratio is no longer $\frac{L_{qq}}{L_{dd}}$ but instead the ratio between the major and minor inductance.

The general inductance saliency ratio including machines subject to cross saturation is then defined to

$$S_L \quad \equiv \quad \frac{L_{\text{major}}}{L_{\text{minor}}}, \tag{9}$$

where the major and minor inductance are functions of dq-currents and rotor position so the saliency ratio becomes a function of dq-currents and rotor position.

From the flux linkage function (3) the saliency ratio and angle can be determined using SVD as described above and here represented by the following functions

$$S_L \quad = \quad S_L(i_d, i_q, \theta_r) \tag{10}$$

$$\theta_L \quad = \quad \theta_L(i_d, i_q, \theta_r) \tag{11}$$

The behaviour of θ_L is of particular interest since it can not be assumed that the derivatives $\frac{d\theta_L}{di_d}$, $\frac{d\theta_L}{di_q}$ and $\frac{d\theta_L}{d\theta_r}$ are zero, which is the typical case for a mechanical position sensor. Hence unexpected behaviour may occur when the position from a position sensor is replaced by a sensorless obtained position. Using the above functions to describe the saliency of the inductances in the machine the suitability for sensorless control relying on inductance may be assessed.

III. Suitability Assessment

The demand to the saliency for sensorless determination of the rotor position are assessed in the following section and the impact on sensorless dq-current control is considered.

Since the ratio and angle represented by (10) and (11) are functions of the current and rotor position some conditions exists which needs to be fulfilled to determine the unique rotor position θ_r and dq-current.

The following four topics are treated in the assessment.

- A Saliency ratio
- B Saliency direction
- C Spacial harmonic disturbance
- D Closed loop control behaviour

A. Saliency Ratio

To track the saliency direction the saliency ratio has to be strictly greater than one. Depending on the distortion of injection signals, typically included in the duty cycle modulation of an inverter supplying the machine and the signal/noise level of the phase current measurements, a minimum saliency ratio $S_{L\text{min.}}$ should be chosen to detect a reliable saliency direction.

The following inequality should be fulfilled for a dq-current trajectory and surroundings where some torque control strategy operates e.g. the MTPA strategy which is intended for low and zero speed. [10]

$$S_L(i_d, i_q, \theta_r) \quad \geq \quad S_{L\text{min.}} \tag{12}$$

If the above inequality holds for all θ_r within a confined dq-current space including a selected torque strategy sufficient saliency is present to detect the direction. In [11] similar analysis of the saliency ratio is conducted to locate the feasible region for sensorless control. However it seems that the used ratio is $\frac{L_{qq}}{L_{dd}}$ which may affect the resultant feasible region if cross saturation is present.

B. Saliency Direction

In case the saliency direction is misaligned with the angle of the dq-frame θ_r by θ_L there may be some unfortunate behaviour depending on what the sensorless obtained position is used for.

If the direction is used as feedback for position control the consequence must be that the controlled position is directly affected with an error of θ_L.

Drives may use closed loop dq-current control to maintain certain torque. The dq-current control is done using the rotor position to transform the signals back and forth between stator and dq-frame values. This kind of control is indirect torque control where a torque reference is translated in to dq-current references based on the used torque strategy. Using the saliency direction with a possible misalignment of θ_L the currents kept by the closed loop controller will be different from the expected and lead to a torque error, which could give an unacceptable loss of rated torque. Using injection methods for low speed, one torque control strategy is the MTPA which has the advantage that

$$\frac{dT_e}{d\theta_i} = 0, \tag{13}$$

where θ_i is the current angle (16) and T_e is the electrical torque. Thus, operating on the MTPA dq-current trajectory, the demand to the accuracy of the current angle can be reduced due to the low impact on the torque T_e.

C. Spacial Harmonic Disturbance

From the saliency direction in (11) there is a mean value across one period of θ_r for a given dq-current. The mean value can be thought of as an offset in the sensorless obtained position. Besides the mean value of θ_L there may exist an additional harmonic disturbance.

For the rotor position to be uniquely identified from the saliency direction, following inequality must be satisfied for a confined operating dq-current region

$$\frac{d\theta_{\hat{r}}}{d\theta_r} > 0, \tag{14}$$

where $\theta_{\hat{r}} = \theta_r + \theta_L$. The consequence is that two different rotor positions will not give the same estimated position at the same dq-current. This means that the demand to the saliency angle θ_L using (8) becomes

$$\frac{d\theta_L}{d\theta_r} > -1. \tag{15}$$

This corresponds to the function $\theta_{\hat{r}}(i_d, i_q, \theta_r)$ for a fixed dq-current is monotonic strictly increasing. Which implies that the inverse function exists so the exact rotor position can in principle be determined from the saliency direction. In practise the material, production tolerances and temperature variations for hybrid machines will most likely mean that obtaining the exact position is too ambitious. Hence in practise compensation for the mean value of θ_L could be performed and the spacial harmonic disturbance is left as an error. The harmonic disturbance could be characterised as a $\pm$ value around the mean value enclosing the error due to harmonic disturbance.

The spacial disturbance considered due to $\frac{d\theta_L}{d\theta_r} \neq 0$ were assessed in this subsection and the remaining assessment is analysing the consequences of non-zero $\frac{d\theta_L}{di_d}$ and $\frac{d\theta_L}{di_q}$ derivatives which is conducted in the following.

D. Closed Loop Control Behaviour

To have control of the dq-current angle θ_i using sensorless dq-current control that uses the obtained position $\theta_{\hat{r}}$ for reference frame transformation, there may exist additional constraints on the behaviour of θ_L.

The angle of the current is given by

$$\theta_i = \angle(i_d + j i_q) \tag{16}$$

$$\theta_{\hat{i}} = \theta_i - \theta_L, \tag{17}$$

where θ_i is the current angle in the dq-frame and $\theta_{\hat{i}}$ is the angle of the same current in the saliency direction frame.

To have control of the dq-current angle θ_i by controlling $\theta_{\hat{i}}$ there should be a unique relation between $\theta_{\hat{i}}$ and θ_i which require the following inequality to be fulfilled, similar to (14)

$$\frac{d\theta_{\hat{i}}}{d\theta_i} > 0. \tag{18}$$

Using (17) this corresponds to

$$\frac{d\theta_L}{d\theta_i} < 1, \tag{19}$$

which can be expressed as $\frac{d\theta_L}{di_d}\frac{di_d}{d\theta_i} + \frac{d\theta_L}{di_q}\frac{di_q}{d\theta_i} < 1$, so the derivative can be found from the function $\theta_L(i_d, i_q, \theta_r)$. In [12] the impact due to cross saturation is studied, and similar interesting considerations are briefly noticed regarding $\frac{d\theta_L}{d\theta_i}$.

If (19) is not satisfied within the desired operating region of the machine the dq-current can not be uniquely determined, hence dq-current control is not possible in the whole region.

E. Summary

To use a machine for sensorless control relying on tracking the saliency direction is a known approach. When using the saliency direction, which depends to some extend on the dq-current and rotor position there may emerge a coupling to the saliency angle θ_L, which could make it impossible to apply sensorless control for a particular machine.

In the assessment 4 topics has been presented. First a sufficient saliency ratio should be present and the position error may be evaluated for the application as described in subsection A and B. Secondly the possible coupling between the saliency angle with the dq-currents and rotor position may be more

critical if there is no unique relation between the estimated angles $\theta_{\hat{r}}$ and $\theta_{\hat{i}}$ to the actual angles for a particular position of the rotor and current as described in subsection C and D.

IV. Analysis Example

A low voltage 12 kW hybrid prototype machine, with 4 pole pairs and 48 stator slots is used in the example. In Fig. 2 and 3 the flux linkage contours is shown, which is the source data. However only the flux linkage average across all positions are shown in the contours.

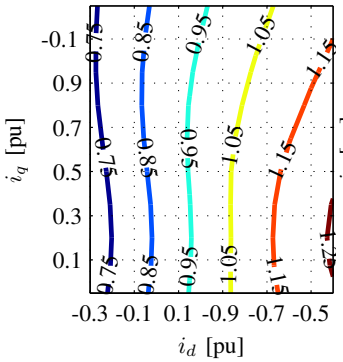

Fig. 2. D-axis flux linkage λ_d [pu].

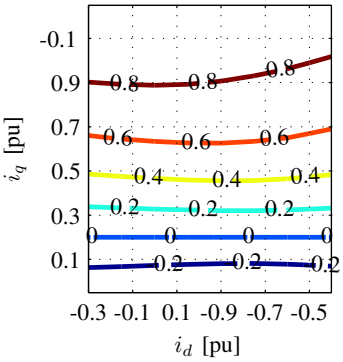

Fig. 3. Q-axis flux linkage λ_q [pu].

A. Flux-linkage Mapping

The flux linkage data (Fig. 2 and 3) is obtained from a batch of finite element model solutions varying the rotor position and dq-current. The data can be considered as a flux-linkage map for the machine, here with a resolution of 10 different q-axis currents, 9 d-axis currents and 48 positions for one electrical period, in total the map consists of 4320 dq-flux linkage values. To obtain an intermediate flux linkage between known values in the map, cubic spline interpolation is used along the d- and q-axis and an intermediate position is obtained using Fourier analysis and synthesis equivalent to sinc interpolation, to provide the ideal reconstruction of the periodic flux linkage. Cubic splines are used so the flux linkage is continuous to the second degree, corresponding to the variation of inductance is continuous.

From the flux linkage contours is it observed that cross inductance is present since the contours are not vertical and horizontal, the cross inductance will give an impact on the saliency angle so it becomes non-zero.

To obtain the saliency direction and ratio, the inductance has to be determined by computing the flux linkage derivatives in (4). Discrete differentiation is not applied to obtain the inductance matrix $\boldsymbol{L}(i_d, i_q, \theta_r)$ for a point, but the derivatives are computed from the cubic spline piecewise polynomial coefficients. For each inductance matrix the saliency ratio and direction are computed using SVD and thereby creating the ratio and angle map where the average contours is shown in Fig. 4 and 5.

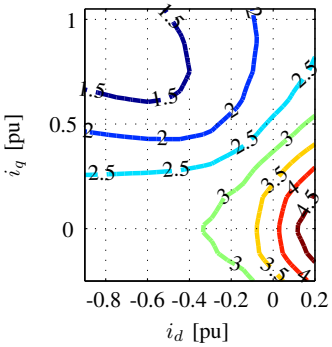

Fig. 4. Saliency ratio S_L [·].

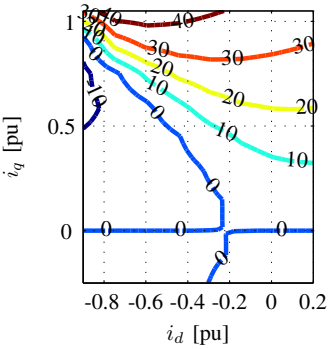

Fig. 5. Saliency angle θ_L [°].

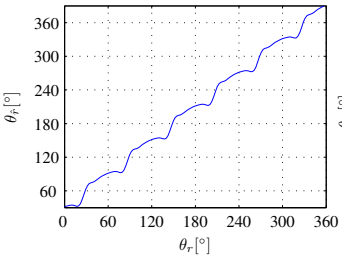

Fig. 6. Sal. direction $\theta_{\hat{r}}$ (sat.).

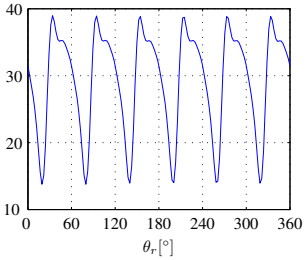

Fig. 7. Sal. angle θ_L (sat.).

B. Saliency Angle

In the analysis example is it observed in Fig. 4 that the saliency ratio is reduced from 4 to below 1.5 at high currents ($i_d = -0.6$pu, $i_q = 0.9$pu). Besides the saliency angle becomes more sensitive to the angle of the current θ_i at high current magnitude, changing fast from $40°$ to $-10°$ in Fig. 5.

In Fig. 6 and 7 the direction and angle is shown for $i_d = -0.6$pu, $i_q = 0.9$pu. In Fig. 6 is it observed that the rotor position can be difficult to determine for some positions. Because the inequality (14) does not hold.

Also the average offset is about $25°$ with a variation of $\pm 14°$.

C. Current Angle

The closed loop behaviour hence the ability to control the real dq-current angle θ_i by controlling the current angle in the estimated frame $\theta_{\hat{i}}$ is shown in Fig. 8 with a dq-current magnitude of $0.9\,\mathrm{pu}$. In Fig. 9 the corresponding saliency angle is shown.

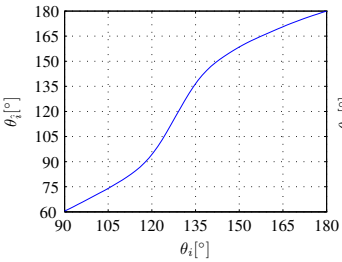

Fig. 8. Current angle $\theta_{\hat{i}}$ (sat.).

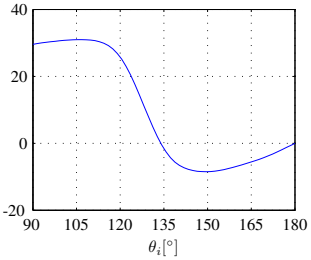

Fig. 9. Sal. angle θ_L (sat.).

Here there is a apparent unique relation between $\theta_{\hat{i}}$ and θ_i so for this case the dq-current angle θ_i can be determined

uniquely from the estimated angle $\theta_{\hat{i}}$ fulfilling inequality (18). However in principle there could exist some rotor positions where this is not the case, since this is the average characteristic.

V. Experimental Results

The experimental results are obtained using a real-time system with a sampling frequency of 5 kHz. The voltage is applied using an PWM inverter equipped with MOSFET's and a dead-time of 2 μs. The phase currents are measured using closed loop hall sensors and sampled in synchronism with the PWM. The purpose of the performed experiments is to study and compare the detailed sensorless characteristics at high-current levels.

A. Methodology

In case the flux linkage map of the machine is determined accurately from measurements, could such a map replace the map obtained based on finite element solutions, and the inductance saliency characteristics be directly compared. In principle it is challenging to measure the flux linkage including harmonics if no sense coils are present. For this reason the impedance saliency characteristics are determined injecting a rotating voltage vector with an amplitude of 2 V and a frequency of $f_i = 500$ Hz in the stator fixed reference frame. The fundamental dq-current is kept in place by PI dq-current control with a bandwidth of $BW \approx 40$ Hz so the injection signal is not attenuated. The rotor speed is fixed to $f_r = 0.8$ Hz (12 rpm) by an external machine.

In principle the inductance and impedance saliency characteristics are not equal due to the resistance, but if the reactance is dominating ($2\pi f_i L \gg R$) the characteristics of the impedance is assumed to be equivalent to the inductance.

The saliency direction is obtained solely from the measured current which can be described by

$$I_{\alpha\beta} = I_{\text{fund.}} e^{j\omega_r t} + I_p e^{j\omega_i t} + I_n e^{-j\omega_i t + j2\theta_{\hat{r}}(t)}, \qquad (20)$$

where $I_{\text{fund.}}$ is the fundamental current at 0.8 Hz and I_p and I_n are the positive and negative frequency component caused by the injection [13].

The saliency direction $\theta_{\hat{r}}(t)$ is half the phase difference between the positive and negative frequency component. The saliency direction is extracted using a 10. order Butterworth low-pass filter with a cutoff frequency of 100 Hz extracting the positive and negative component using frequency shifting. Finally the direction is found from the angle of the multiplied components.

$$\theta_{\hat{r}} = \frac{1}{2} \angle I_p I_n e^{j2\theta_{\hat{r}}(t)}. \qquad (21)$$

The good properties of the method is insensitivity to the inherent phase shift in the low-pass filter and delays in the current sampling which else could affect the extracted saliency direction.

To establish the saliency ratio of the impedance characteristic the magnitude of the positive and negative frequency component are used [14]

$$S_Z = \frac{I_p + I_n}{I_p - I_n}. \qquad (22)$$

Considering the equation (20) the trajectory outline is an ellipse profile with the centre in $I_{\text{fund.}} e^{j\omega_r t}$ with an average radius of I_p varying with $\pm I_n$ between the major and minor axis, hence the saliency ratio of an ellipse.

B. Saliency Direction

The experimentally determined saliency direction is shown in Fig. 10, 12 and 14 for different d-axis currents but with a fixed q-axis current of $I_q = 0.9$ pu.

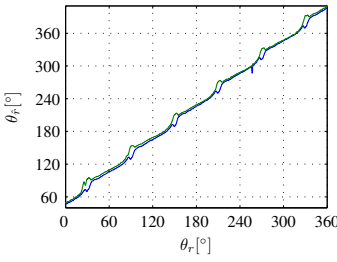

Fig. 10. Sal. dir. $\theta_{\hat{r}}$, $I_d = -0.5$ pu.

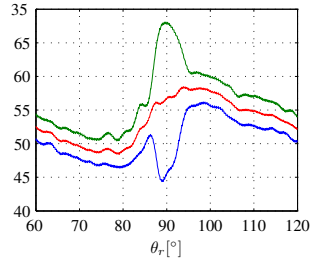

Fig. 11. Sal. angle θ_L, $I_d = -0.5$ pu.

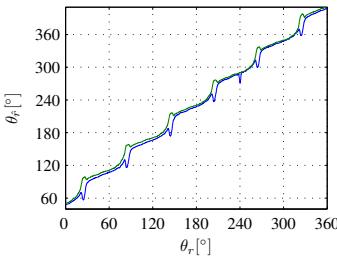

Fig. 12. Sal. dir. $\theta_{\hat{r}}$, $I_d = -0.6$ pu.

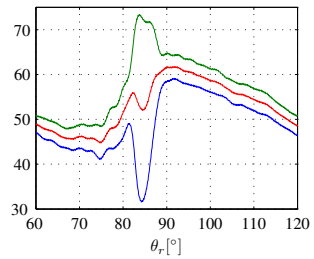

Fig. 13. Sal. angle θ_L, $I_d = -0.6$ pu.

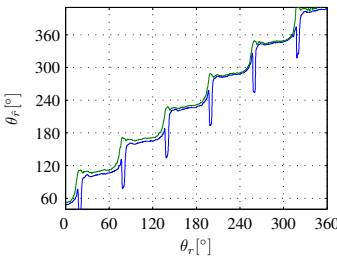

Fig. 14. Sal. dir. $\theta_{\hat{r}}$, $I_d = -0.7$ pu.

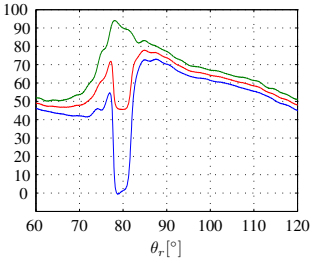

Fig. 15. Sal. angle θ_L, $I_d = -0.7$ pu.

The upper and lower curves in each figure are the determined saliency direction using -500 Hz and $+500$ Hz as injection frequency respectively. The difference in the two curves is caused by the resistance in the machine, hence the difference between the saliency characteristic of the impedance at $+500$ Hz and -500 Hz. Comparing Fig. 12 with the one obtained based on finite element data (Fig. 6) there are 6 distinct notches at the similar rotor positions. At the notch

position the difference between using an positive or negative injection signal is remarkable. The reason for the increased difference is the saliency ratio is reduced close to one at those rotor positions, increasing the impact from the resistance.

In Fig. 13 the corresponding saliency angle is shown in detail for one notch. The upper and lower line corresponds to the angle obtained using $-500\,\mathrm{Hz}$ and $+500\,\mathrm{Hz}$ as injection frequency. The line in-between is the average of the two. The average offset in the saliency angle is $53°$ instead of $25°$ obtained from the finite element data, and the variation is $\pm 8°$ instead of $\pm 14°$.

In Fig. 10 and 14 the d-axis current are changed, which gives an impact on the notch phenomena. At a reduced d-axis current the notch magnitude is reduced and the saliency direction is close to monotonic. Increasing the d-axis current the saliency direction characteristic becomes quite unattractive due to the more or less rough stair case shape.

Observing the notch behaviour in Fig. 11, 13 and 15, the location of the notch is not fixed at the same rotor position, but moves to the left increasing the d-axis current magnitude.

The remarkable difference between $+500\,\mathrm{Hz}$ and $-500\,\mathrm{Hz}$ at the notch locations can be explained due to a decreased saliency ratio which is shown in Fig. 16, 17 and 18.

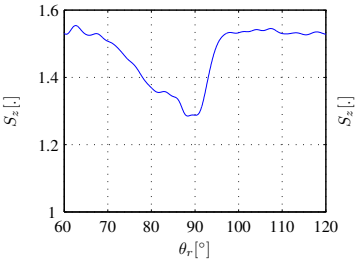

Fig. 16. Sal. ratio S_z, $I_d = -0.5$ pu

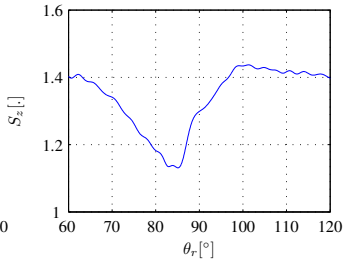

Fig. 17. Sal. ratio S_z, $I_d = -0.6$ pu.

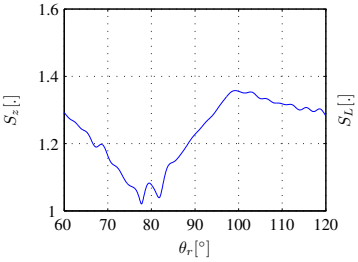

Fig. 18. Sal. ratio S_z, $I_d = -0.7$ pu.

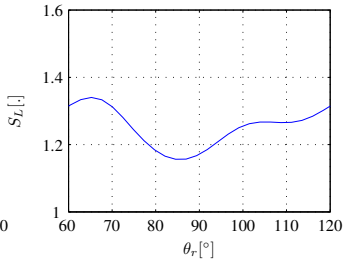

Fig. 19. Sal. ratio S_L, (sat.).

Comparing the ratio in Fig. 17 with the one based on finite element data in Fig. 19 there is some agreement of the value and location of the minimum saliency. Furthermore in Fig. 18 with the high d-axis current it is noticed the ratio is very close to one, so the angle in this position is quite uncertain.

C. Current Angle

In Fig. 20 and 21 the determined current angle is shown comparable to Fig. 8 and 9. The measured upper and lower characteristic in Fig. 21 shows the result using an injection

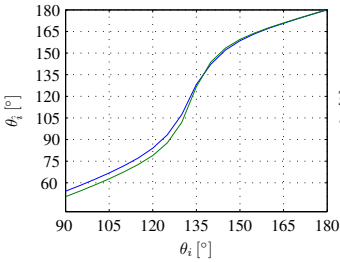

Fig. 20. Current angle $\theta_{\hat{i}}$ (meas.).

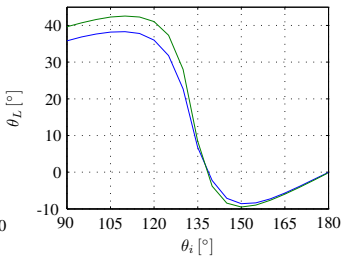

Fig. 21. Sal. angle θ_L (meas.).

frequency of $-500\,\mathrm{Hz}$ and $+500\,\mathrm{Hz}$ respectively. The difference between the positive and negative characteristic at a low current angle is caused by an increased impact of the resistance. The current angle has a quite similar behaviour with the one obtained based on finite element data and there is a maximum of $43°$ and a minimum of $-10°$.

.

VI. Discussion

The analysis method proposed is based on the flux linkage functions $\lambda_d(i_d, i_q, \theta_r)$ and $\lambda_q(i_d, i_q, \theta_r)$. The tolerances on those functions may influence the analysis results in particular $\frac{d\theta_L}{d\theta_i}$ because differentiation is done twice. First differentiation by the dq-currents to obtain the inductance matrix, and again after the matrix decomposition to get $\frac{d\theta_L}{d\theta_i}$. Using the finite element based flux linkage map the tendencies of the saliency direction and current angle is in good agreement with the experimental obtained results. However the absolute values of the saliency ratio and angle are in less agreement.

VII. Conclusion

Replacing a mechanical sensor with sensorless injection based methods that use the hybrid PM machine as a self sensing device is at first hand attractive. But considering practical phenomenons like magnetic saturation and spacial harmonics, not all machine designs will be equally suited for sensorless operation and a comprehensive analysis is required to determine the suitability.

In this paper machine flux linkages are introduced as function of currents and rotor position, which result in an analysis of sensorless characteristics described by saliency ratio and angle.

To have a machine suitable for sensorless control, the two inequalities

$$\frac{d\theta_L}{d\theta_r} > -1 \qquad \text{and} \qquad \frac{d\theta_L}{d\theta_i} < 1$$

should be fulfilled in the desired operating region.

Some machines may be directly suitable for sensorless control, other perhaps need some compensation scheme for the offset in the saliency angle and some machines may have unfortunate characteristics in some operating regions where sensorless control becomes difficult.

REFERENCES

[1] C. Chan, K. Chau, J. Jiang, W. Xia, M. Zhu, and R. Zhang, "Novel permanent magnet motor drives for electric vehicles," *IEEE Trans. Ind. Electron.*, vol. 43, no. 2, pp. 331–339, 1996.

[2] M. J. Corley and R. D. Lorenz, "Rotor position and velocity estimation for a salient-pole permanent magnet synchronous machine at standstill and high speeds," *IEEE Transactions on Industry Applications*, vol. 34, no. 4, pp. 784–789, Jul./Aug. 1998.

[3] J.-I. Ha, K. Ide, T. Sawa, and S.-K. Sul, "Sensorless rotor position estimation of an interior permanent-magnet motor from initial states," *IEEE Transactions on Industry Applications*, vol. 39, no. 3, pp. 761–767, May/Jun. 2003.

[4] M. Schroedl and P. Weinmeier, "Sensorless control of reluctance machines at arbitrary operating conditions including standstill," *IEEE Trans. Power Electron.*, vol. 9, no. 2, pp. 225–231, 1994.

[5] S. Shinnaka, "New "mirror-phase vector control" for sensorless drive of permanent-magnet synchronous motor with pole saliency," *IEEE Transactions on Industry Applications*, vol. 40, no. 2, pp. 599–606, Mar./Apr. 2004.

[6] A. Piippo, M. Hinkkanen, and J. Luomi, "Sensorless control of PMSM drives using a combination of voltage model and HF signal injection," in *Industry Applications Conference, 2004. 39th IAS Annual Meeting. Conference Record of the 2004 IEEE*, vol. 2, Oct. 2004, pp. 964–970.

[7] J. Holtz, "Acquisition of position error and magnet polarity for sensorless control of pm synchronous machines," *IEEE Trans. Ind. Appl.*, vol. 44, no. 4, pp. 1172–1180, 2008.

[8] B. Stumberger, G. Stumberger, D. Dolinar, A. Hamler, and M. Trlep, "Evaluation of saturation and cross-magnetization effects in interior permanent-magnet synchronous motor," *IEEE Transactions on Industry Applications*, vol. 39, no. 5, pp. 1264–1271, Sep./Oct. 2003.

[9] T. Matzen and P. Rasmussen, "Modelling magnetic saturation effects in ipmsms for use in sensorless saliency based methods," in *Proc. European Conference on Power Electronics and Applications*, 2007, pp. 1–8.

[10] M. Uddin, T. Radwan, and M. Rahman, "Performance of interior permanent magnet motor drive over wide speed range," *IEEE Transaction on Energy Conversion*, vol. 17, no. 1, pp. 79–84, 2002.

[11] N. Bianchi, S. Bolognani, J.-H. Jang, and S.-K. Sul, "Advantages of inset pm machines for zero-speed sensorless position detection," *IEEE Trans. Ind. Appl.*, vol. 44, no. 4, pp. 1190–1198, 2008.

[12] P. Guglielmi, M. Pastorelli, and A. Vagati, "Cross-saturation effects in ipm motors and related impact on sensorless control," *IEEE Trans. Ind. Appl.*, vol. 42, no. 6, pp. 1516–1522, Nov.–dec. 2006.

[13] H. Kim and R. D. Lorenz, "Carrier signal injection based sensorless control methods for IPM synchronous machine drives," in *Industry Applications Conference, 2004. 39th IAS Annual Meeting. Conference Record of the 2004 IEEE*, vol. 2, Oct. 2004, pp. 977–984.

[14] T. Matzen and M. M. Bech, "Sensorless control of IPMSM by voltage injection," in *Proceedings of the Nordic Workshop on Power and Industrial Electronics (NORpie)*, Jun. 2006.